https://doi.org/10.5194/nhess-2022-195
Preprint. Discussion started: 11 July 2022

Natural Hazards and Earth System Sciences
Open Access
Discussions

Assessment of Short-medium Term Intervention Effects Using CAESAR-Lisflood in Post-earthquake Mountainous Area

Di Wang[1,2,3], Ming Wang[1], Kai Liu[1]

[1]School of National Safety and Emergency Management, Beijing Normal University, Beijing, China.

[2]Academy of Disaster Reduction and Emergency Management, Beijing Normal University, Beijing, China.

[3]Faculty of Geographical Science, Beijing Normal University, Beijing, China.

Correspondence to: Ming Wang (wangming@bnu.edu.cn)

Abstract

The 2008 Wenchuan earthquake triggered local geomorphic changes rapidly and gradually and produced abundant materials through external processes. The abundant materials increased the risks of geomorphic hazards (flash floods, landslides, and debris flows) induced by extreme precipitation in the area. To reduce sediment transport present in geomorphic hazards, intervention measures such as dams, levees, and vegetation revetments have been constructed in specified sites.

This study concentrated on the assessment of intervention effects incorporated with various facilities on post-earthquake fragile mountains in the short-medium term. Take the Xingping valley as an example, we used the CAESAR-Lisflood landscape evolution model to simulate three different scenarios including unprotected landscapes, present protected landscapes, and enhanced protected landscapes in 2011-2013. We compared the geomorphic changes and defined two indicators to assess the intervention effects.

https://doi.org/10.5194/nhess-2022-195
Preprint. Discussion started: 11 July 2022

The results showed that the mitigation facilities were effective, especially engineering measures that cooperated with vegetation revetments in the upstream area, and the present mitigation measures were inadequate to stop materials loss and prevent hazards from the upstream area. Moreover, the effectiveness reduced gradually caused by the storage capacity of dams decreased. The simulation methods assessed the ability and effectiveness of cooperated control measures and could support optimum mitigation strategies.

1. Introduction

Strong earthquake shaking fractures rock mass; the resulting cracks are propagated into a weak plane (Huang, 2009) by weathering and erosion; the resulting source materials increase in mountainous regions, and modify mountain landscapes by various surface processes for days, years, and millennia (Fan et al., 2019). That means the quake-stricken areas will trigger landslides (a general term to describe the downslope movement of soil, rock, and organic materials under the influence of gravity and also the landform that results from such movement) by complicated processes. The devastating earthquake measuring Ms =8.0 (the surface-wave magnitude which is the logarithm of the maximum amplitude of ground motion for surface waves with a wave period of 20 seconds) that struck the Wenchuan area has produced landslides that threaten highways, railways, towns, and other infrastructure. Although limited comprehensive mitigation measures were constructed in potentially dangerous sites, disasters still occurred because of complex processes and origins, high-frequency precipitation, and the low cost of treatment (Cui et al., 2013; Yu et al., 2010). Therefore, understanding intervention measures is crucial for effective mitigation. More studies mainly focus on the establishment of post-evaluation effectiveness index systems

https://doi.org/10.5194/nhess-2022-195
Preprint. Discussion started: 11 July 2022

without more practices (N. Wang et al., 2015; L. Zhang and Liang, 2005) and long-term measurement of changes before and after mitigation measurement by field surveys (Chen et al., 2013; Zhou et al., 2012). The subjective expression determines that the index system establishment is still in the theoretical stage and the measurement cost is high in time and money. Recent research compares the disaster characteristics before and after the intervention, which are quickly obtained from disaster simulation (Cong et al., 2019). While the characteristics express the process ignoring the long time effects on the geomorphic changes. Thus, the short-medium term and spatial geomorphic changes quickly obtained from the simulation will provide more details to interpret engineering measures in special sites even in those inaccessible to humans.

The open access 2-D landscape evolution model CAESAR-Lisflood (C-L) is based on Cell Automata (CA) framework, which has powerful spatial modeling and computing capabilities to simulate complex dynamic systems (Batty et al., 1997; Batty and Xie, 1997; Couclelis, 1997), enables the study of many earth system interactions with different environmental forces. Representation of deposition and erosion within C-L is used widely in rehabilitation planning and soil erosion predictions from a post-mining landform (Hancock et al., 2017; J.B.C.Lowry et al., 2019; Saynor et al., 2019; Slingerland et al., 2019; Thomson and Chandler, 2019) and channel evolution and sedimentary budget in dam settings (Gioia and Schiattarella, 2020; Poeppl et al., 2019). In addition, there have been a series of studies in the mountainous area involving secondary geo-hazard driving factors (Li et al., 2018; M. Wang, Liu, et al., 2014) and vegetation recovery (X. Zhang et al., 2018). C-L was used with different scenarios of rainfall or future climate change to interpret the landscape evolution after the Wenchuan earthquake (Li et al., 2020; Xie et al., 2018). The methods and parameters values used in the above research helped to promote the application in other study areas.

https://doi.org/10.5194/nhess-2022-195
Preprint. Discussion started: 11 July 2022

In this study, we compared the short-medium term scenario simulations to assess the effectiveness of a set of mitigation facilities and to analyze the role of each measure in the specific site. The results will guide the control of secondary geological disasters after an earthquake.

2. Study area

2.1 *Regional characteristics*

The study area was Xingping valley in the northeastern Sichuan province, a left branch of the Shikan River (a tributary of the Fu River) (Fig. 1). There are nearly two hundred households scattered among more than five villages in the catchment. The topography of the catchment is rugged with an elevation between 800 and 3036 m and an area of approximately 14 km^2. The catchment shape looks like a "leaf" with a nearly U-shaped main ditch characterized by a high longitudinal gradient (~ 120‰) and more than ten small V-shaped branch gullies. The length from northeast to southwest is 5770 m, the other direction perpendicular to which is 4150 m. The region is characterized by a humid temperate climate with a mean annual temperature of 14.7℃. The mean annual precipitation is up to 807.6 mm with maxima between May and September. The steep terrain and short-term heavy rainfall make an ephemeral stream in this area.

The geological settings are mainly distributed metamorphic sandstones, sandy slate, crystalline limestone, and phyllite of Triassic Xikang Group (T_{3xk}) and Silurian Maoxian Group (S_{mx}), which easily induce a large amount of loose solid material after weathering of a static process. Wenchuan earthquake, a dynamic process made this area one of the most severely affected locations with a Modified Mercalli Intensity scale of IX and X (M. Wang, Yang, et al., 2014). The earthquake strengthened the

https://doi.org/10.5194/nhess-2022-195
Preprint. Discussion started: 11 July 2022

Natural Hazards and Earth System Sciences
Open Access
Discussions

solid material produced and reached 10^6 m^3 by triggering landslides and other surficial movements from Mayuanzi, Zhengjiashan, and Wujiaping (Fig. 1)(Guo et al., 2018).

2. 2 *Historical hazards and intervention measures*

To reflect most of the landslides processes in spatial relationships according to the site survey and literature research on the characteristics of the historical hazard, we divided the study area into three regions: source area, translation area, and deposit area (Feng et al., 2017; Guo et al., 2018; Zhao et al., 2019) (the dashed lines in Fig. 1. (c)). The loose solid materials induced by severe rain are easily motivated from the source area to the deposit area through the translation area. There burst 6 group debris flow-flash flood disaster chains in rainfall season according to field surveys. Table 1 shows the occurred time, total rainfall of each period, corresponding disaster description, and landslides distribution delineated from remote sensing image data.

https://doi.org/10.5194/nhess-2022-195
Preprint. Discussion started: 11 July 2022

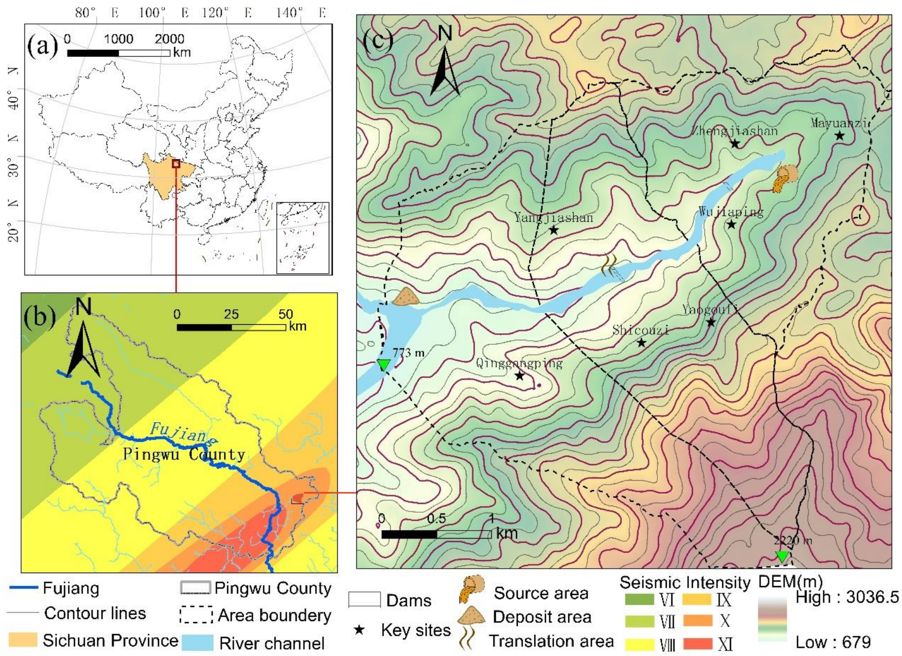

Fig. 1 The location of the study area. (a) Location within China. (b) Location within the seismic intensity ranges of the Wenchuan earthquake. (c) The spatial relationship of the source area, translation area, deposit area, and distribution of elevation.

Table 1 History of hazards in the study area

Time	Total rainfall (mm)	Details	Landslides distribution
2008.9.24	140.0	The debris flows after the earthquake first broke out from Mayuanzi and the deposited sediment was up to 5.0×10^4 m^3 at the junction with the Shikan river, which resulted in collapsed houses and a mess of farmland in the inundation. *	/
2009.7.15-7.16	200.0	The debris flow erupted for 20 min and carried 2.5×10^4 m^3 solid materials into the outlet section in the catchment. *	/
2010.8.13	223.3	Loose materials were carried from branch outlets into the main outlet and deposited in their routes. *	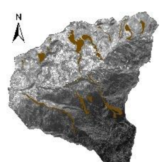
2011.8.20	118.0	The scenario was like in 2010.8.13, while damaged less. *	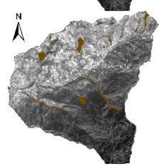

https://doi.org/10.5194/nhess-2022-195
Preprint. Discussion started: 11 July 2022

Natural Hazards and Earth System Sciences Discussions

2013.7.7-7.12	800.0	The landslides occurred in the upper steep branch, turning to a rapid and large flow-like motion in the main outlet and sweeping over the houses, pigsty, and arable land near the channel. Eventually, the mixture of soil and fragmented rocks accumulated 29.5×10^4 m^3. *	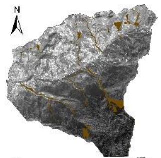
2018.7.9-7.11	360.0	Several branches burst debris flows, and the materials from Qing-gangping accumulated on the road more than 2 m. *	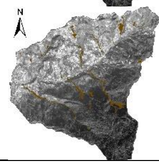

*means the sources are mainly from literature research (Feng et al., 2017; Guo et al., 2018; Zhao et al., 2019)

Vulnerability to landslide hazards is a function of a site's location (topography, geology, drainage), type of activity, and frequency of past landslides (Highland and Bobrowsky, 2008). Consequently, this landscape will not stop experiencing landslide hazards in the short term. To stabilize the loose solid materials, an engineering control project was completed in October 2010. The project included two blocking dams, one of which was in the upper source area and the other in the translation area (Feng et al., 2017)(Fig. 1(c)). The storage capacity of the two reservoirs are, respectively, 5.78×10^4 m^3 and 7.2×10^4 m^3 and the upper dam (10.0 m) is higher than the other one (9.0 m). With deposited in the reservoirs gradually, the first dredging work was after landslide hazards in 2013 and the upper reservoir remained at half capacity in 2016, meanwhile, the lower reservoir was full of loose material.

3. Materials and Methods

3.1 Scenarios settings

The abundant source materials of landslides are provided in the quack-stricken area. Control processing should be performed to prevent the transportation of loose solid materials. We simulated three scenarios incorporating engineering measures and biological measures to assess the geomorphic response in 2011-2013 and then as-

https://doi.org/10.5194/nhess-2022-195
Preprint. Discussion started: 11 July 2022

sessed the effectiveness of intervention measures. Scenario UP: Unprotected landscapes, which means the sediment will move with no anthropogenic intervention. Scenario PP: Present protected landscapes, the present two blocking dams stop a large amount of material from moving downslope in 2011-2013 without dredging work all the time (see section 2.2). Scenario EP: Enhanced protected landscapes, the two blocking dams in Scenario PP plus vegetation revetments in the source area and levees in the deposit area. The placement of additional facilities was decided by the annual field survey results, where there are still a large number of materials and the settlements would be damaged every year (see Fig. 2 and Section 3.2.2). The vegetation revetments reduce erosion by enhancing the infiltration capacity of soil and reducing the surface flow velocity. The levees are artificial embankments to protect the plow land and buildings; they are constructed to prevent flow and prevent the mix of water and sediment from overflowing and flooding surrounding areas. We simulated and compared the three types of situations described above.

3.2 C-L model description and setting

The C-L (Tom J Coulthard et al., 2013) was integrated the Lisflood-FP 2D hydrodynamic flow model (Bates et al., 2010) with the CAESAR geomorphic model (T J Coulthard et al., 2002; Van De Wiel et al., 2007), which is based on CA framework to suit the gridded data required in geomorphic processes simulation. Its stronger physical basis in a two-dimensional hydrodynamic flow model and faster simulation in a complete catchment over time scales from hours to thousands of years made it our surface process simulator. The catchment mode requires the surface digital elevation model (DEM), the bedrock DEM, the grain size distribution, the rainfall data and other parameters (Table 2), and related output settings.

https://doi.org/10.5194/nhess-2022-195
Preprint. Discussion started: 11 July 2022

Natural Hazards and Earth System Sciences
Open Access
EGU
Discussions

Besides the creative flow model, which is used to simulate the shorter term hydrodynamic effects, there are three main parts hydrological model, erosion and deposition model, and slope progress. The hydrological model uses input rainfall data to generate runoff in the catchment based on adaption of TOPMODEL (Topography based hydrological model) (Beven and Kirkby, 1979), which is routed in flow model including velocity and depth, which are then used to calculate shear stress that can then be used to calculate fluvial erosion and deposition. The slope model enables materials from the slope to be fed into the fluvial system with mass movement occurring when a critical slope threshold is exceeded and soil creep as a function of the slope. These models update variables in square gridded cells at any time interval, such as elevation and derived topographic data, grain sizes and proportion data, hydrological data (e.g., discharge, water depth, velocity), and other types of generalization data.

For three different scenarios, we reconstructed four parameters formatted differently in catchment mode such as DEM, bedrock DEM, M, and rainfall series. The arrangements of the input parameters are described as follows.

3.2.1 Surface and bedrock digital elevation model

Although the run time of the C-L simulation increases exponentially as the number of grid cells increases, to describe clearly the control process, especially the two dams and levees in the catchment, we unified grid cell scales to 10 m for all needed data. The GlobalDEM product with a 10 m × 10 m resolution and 5 m (absolute) vertical accuracy was used as the prepared data to form three types of initial DEMs (UP DEM, PP DEM, and EP DEM). Before rebuilding initial DEMs, we filled the sinks of the original GlobalDEM, which were prone to form by interpolation operation, and then caused the hydrological module to calculate inconsequently. The DEM could be used as the surface DEM of the unprotected landscapes (UP DEM) in 2011. According to the engineering control project described in Section 3.2.2, present protected landscapes' surface DEM (PP DEM) was added 10 m and 9 m in the location of dams, respectively. Similarly, the enhanced protected landscapes' surface DEM (EP DEM) was extracted by increasing the value of specified grid cells which would be expressed levees building based on PP DEM. And the height of the levees was 2 m, an average height used in the lower river channel of the study area to prevent high and fast flow.

From the field survey and the contents of section 2.2, the spatial distribution of erodible thickness (the difference between surface DEM and bedrock DEM) was different. The bedrock DEM included in this model for each scenario to stop eroding was derived by subtracting erodible thickness from surface DEM. The distribution of erodible thickness was divided into five regions (Fig. 2) by comparing the foundation of buildings, the exposed bedrock, and the residents' memory of the history of landslides deposited. The average thicknesses of upstream low and high-altitude areas were set to 10 m and 3 m, respectively, and the erodible layer in the downstream area was supposed to be 3 m. For the river channel and outlet, there would be a large amount of deposition and there were supposed to be 5 m and 4 m approximately. The engineering control processes with two dams in Scenario PP and two dams cooperated with levees in Scenario EP were supposed to be non-erosive concrete. So the erodible thickness of the engineering control processes area was 0 m. Fig. 2 shows the flow chart of the generation of DEMs and bedDEMs. In addition, all of the DEM were formatted ASCII raster as required in C-L.

https://doi.org/10.5194/nhess-2022-195
Preprint. Discussion started: 11 July 2022

Natural Hazards and Earth System Sciences Discussions

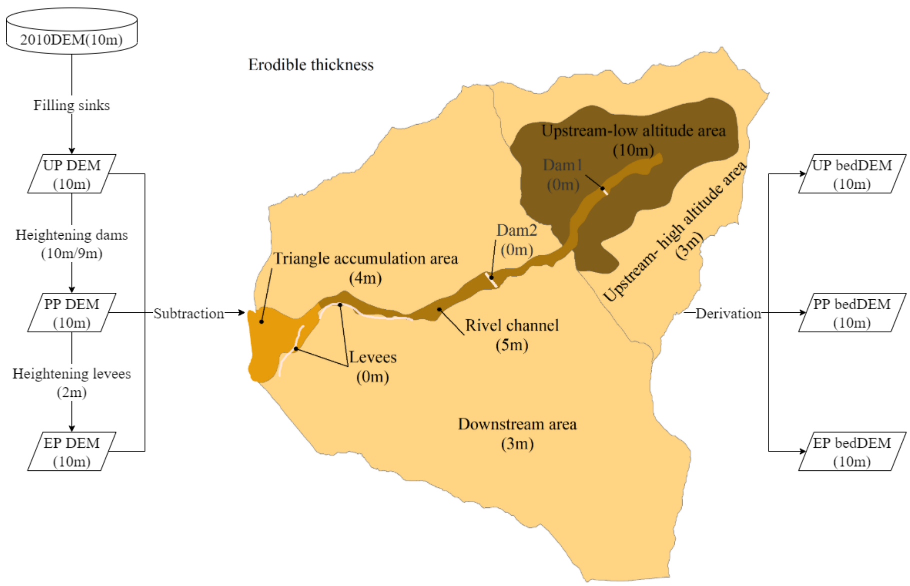

Fig. 2 Flow chart describing the generation of DEMs and bedDEMs (bedDEM: bedrock DEM). All the numbers attached to DEM on both sides indicated the DEM grid's width and the numbers under facilities such as dams on the left one are height measured from surface DEM. The numbers in central erodible thickness are the depth of the material which is capable to remove by runoff.

3.2.2 Vegetation settings

Another parameter in scenarios used in simulations was “m” which controlled the exponential decline of transmissivity with depth (Batty et al., 1997) and influenced the peak and duration of the hydrograph in response to rainfall. The lower the value of “m”, the lower the vegetation coverage, the flashier flood peaks, and the shorter duration hydrographs. In this research, the “m” in UP and PP scenarios were set to 0.008 without spatial variation, which represented that the vegetation coverage is similar to farmland referenced to research in the same study area by Li et al., (2020). As mentioned earlier, the upstream-low attitude area covered by the biological measures designed in the EP scenario indicated a high value of “m”. To distinguish the “m” in the biological protected area clearly, the “m” was set to 0.02, equal to the vegetation coverage in the forest (Li et al., 2020).

3.2.3 Rainfall data

In this research, we compared three scenarios with identical precipitation data during 2011 and 2013 as mentioned in section 3.1. The source data of precipitation in 2011-2013 (Fig. 3(a)) was from the China Meteorological Administration (http://data.cma.cn) with daily temporal resolution. The rainfall intensity and the frequency of extreme events affect patterns of erosion and deposition (Tom J. Coulthard et al., 2012), therefore, we used the stochastic downscaling method to generate hourly data to best capture the hydrological events in this study, which was introduced by Li et al., (2020) and Lee and Jeong, (2014). The referenced hourly precipitation was from the pluviometer located 20 km from the study area in 2016(Fig. 3(b)), with annual total precipitation of 684 mm. The rainfall in 2016 was characterized by (1) hourly precipitation from 1.1 mm to 35.4 mm and (2) the maximum and average duration of a rainfall event up to 24 h and 2.8 h. In the downscaling method, the daily rainfall was divided into four levels (>100 mm, 50-100 mm, 20-50 mm, and 0-20 mm) and the referenced hourly rainfall series of those days whose daily rainfalls were close to the value on the day at a certain level were combined by reproduced, crossed and mutated included in the genetic algorithm (Goldberg, 1989). At last, the downscaled rainfall series were generated by gathering the normalized hourly data based on the daily rainfall. Fig. 3(c) shows the downscaled rainfall series in 2011-2013, which illustrated that the downscaled hourly precipitation series was better than the hourly-mean precipitation (5.27 mm) in the day with maximum precipitation (126.5 mm).

https://doi.org/10.5194/nhess-2022-195
Preprint. Discussion started: 11 July 2022

Natural Hazards and Earth System Sciences
Open Access
EGU
Discussions

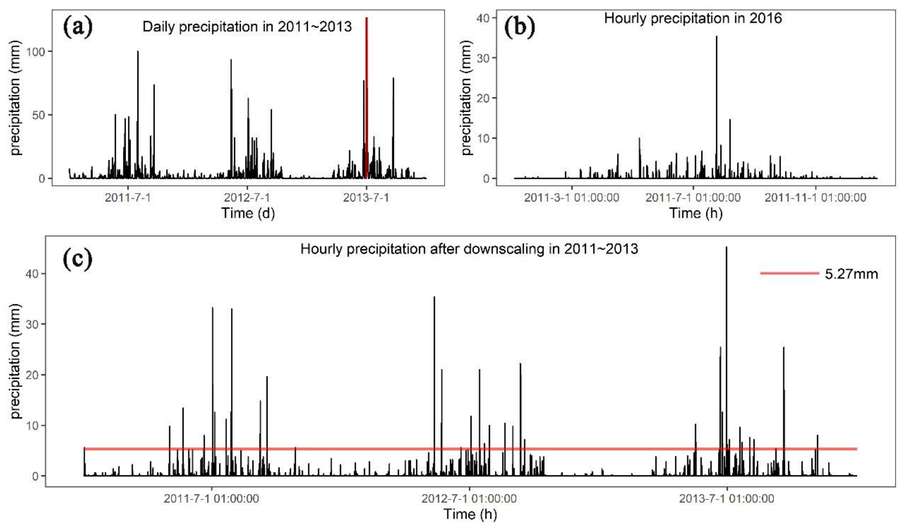

Fig. 3(a) showed the required downscaling daily precipitation in 2011-2013 (the red vertical line indicates daily maximum precipitation of 126.5 mm); (b) showed the referenced hourly precipitation in 2016; (c) showed the downscaled hourly precipitation in 2011-2013 (the red horizontal line indicates the hourly-mean precipitation 5.27 mm in the day with maximum precipitation showed in (a))

3.2.4 Other parameters

The C-L model is sensitive to a set of model physically based parameters included in Skinner et al., (2018) for an identical catchment with a grid cell size of 10 m, such as slope for edge cells, grain size set, vegetation critical shear stress, and Manning's n values. These parameters were determined by the application of Xie et al., (2018) and Li et al., (2020) in the same study area. In particular, the manning n roughness was set according to suggested values (Arcement and Schneider, 1989) in different land-use, and other more sensitive parameters were determined by repeated experiments such as the minimum Q value (see Table 2).

Table 2 The C-L parameter values for the simulations of three different scenarios.

Parameters	Value	Description
9 kinds of grainsizes (m) (grainsize proportion) ★★	0.000074(0.098), 0.0005(0.138), 0.001(0.052), 0.002(0.162), 0.005(0.158), 0.01(0.169),	Used for calculating the sediment transport in each active layer

https://doi.org/10.5194/nhess-2022-195
Preprint. Discussion started: 11 July 2022

Natural Hazards and Earth System Sciences
Open Access
EGU
Discussions

	0.02(0.13), 0.04(0.06), 0.1(0.033)	
Suspended fall velocity(m/s)	0.0003	Designated as the falling velocity for the finest fraction(74μm)
Sediment transport formula ★★★★	Wilcock and Crowe	A criterion calculated the fluvial erosion and deposition for all cells
Max erode limit (m) ★★★	0.002	The maximum amount of material that can be eroded within a cell at each time step
In channel lateral erosion rate ★★★	20	Controlling the channel narrowing
Active layer thickness (m)	0.1	The thickness of a single active layer
Lateral erosion rate ★	0.000003	The variable controls lateral erosion
Lateral edge smoothing passes	40	The number of passes for the edge smoothing filter (distance between two meanders)
Vegetation critical shear stress (Pa) ★★★	100	The value above which vegetation would be removed by fluvial erosion
Grass maturity rate (yr) ★	1	The speed at which vegetation reaches full maturity in years
The proportion of erosion that can occur when vegetation is fully grown	0.1	Determined the effects of vegetation maturity on “in channel lateral erosion rate” and the “lateral erosion rate”.
Soil creep rate(m/yr) ★★	0.0025	The variable tends to cause erosion gradually on sharper features in the terrain
Slope failure threshold (◦) ★★★	60	Angle threshold in degrees above which landslide occur
Input/output difference allowed(m^3/s) ★★	0.5	Described the flow model running in a steady state and used to speed up the model operation
Min Q for depth calculate(m) ★★★	0.1	The value above which the flow depth would be calculated to save running time
Water depth threshold above which erosion will happen(m)	0.01	The value above which the model starts to calculate erosion
The slope for edge cells ★★	0.005	The exit cells’ slope to control the erosion and deposition
Evaporation rate (m/d) ★★★	0.00418	Used to calculate the evapotranspiration
Courant number	0.3	The value controls the numerical stability and speed of operation of the flow model
Mannings n roughness (forest, farmland, landslide, river channels) ★★	0.02, 0.008, 0.003, 0.002	The roughness coefficient used by the flow model

Note: The greater the number of ★, the more sensitive to the model, and the unlabeled parameters were not studied (Skinner et al., 2018).

https://doi.org/10.5194/nhess-2022-195
Preprint. Discussion started: 11 July 2022

3.3 Output analyses

The overall temporal and spatial changes in internal geomorphology under three different scenarios were available to assess intervention measure effectiveness. The simulated elevation changes on the last day of each year were selected to show the details, which were derived from the difference between output DEMs and initial DEMs (EleDiffs). The EleDiffs indicated the depth of sediment deposition or erosion (>0: deposition, <0: erosion). We classified the depth to show the distribution of the deposition and erosion, defined the total damaged area in each scenario by summing all affected cells' areas, and compared the damaged area of every classification in three scenarios. In addition, we zoomed in on the key spots including blocking dams, levees, and vegetation revetments to explore the geomorphic response to various control measures in different scenarios and record the depth of deposition in dams blocking areas. To quantify the changes in the internal source area, translation area, and deposition area, the sediment volumes of deposition and erosion were calculated respectively from the EleDiffs cuboid.

In different scenarios with different intervention measures, the divided regions would behave differently in sediment conservation. To quantify the conservation ability conveniently, we defined some related variables based on the sediment balance system (Fig. 4). In the balance system, for the region n, the deposited sediment (D_n) and the input sediment from the upper connected region (I_n) are equal to the eroded material volume (E_n) plus the output volume to the next region (O_n) in the same period. Based on the relationship between variables shown in Eq.1 and Eq.2, we defined C_a (Eq. 3) to quantify the sediment conservation ability.

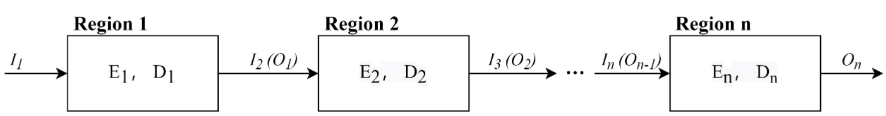

https://doi.org/10.5194/nhess-2022-195
Preprint. Discussion started: 11 July 2022

Natural Hazards and Earth System Sciences Discussions

Fig. 4. The sediment balance system in the study area (the Region *n* indicated source area, translation area, and deposit area in this study)

$$I_n = \sum_{2}^{n} E_{n-1} - \sum_{2}^{n} D_{n-1} \tag{1}$$

$$I_n + E_n = O_n + D_n \tag{2}$$

$$Ca = \frac{D_n}{I_n + E_n} \tag{3}$$

Where n is the region number of source area (=1), translation area (=2), and deposit area (=3).

The daily sediment yield measured in the valley was the other important output variable of sediment transport. We referenced a terminology from the stock market in economics to assess the relative efficiency (Eq. 4, compared with Scenario UP) of engineering protections in scenario PP and engineering cooperation with biological measures in scenario EP.

$$Re_{PP/EP,i} = \frac{Q_{UP,i} - Q_{PP/EP,i}}{Q_{UP,i}} \tag{4}$$

Where i is the sequence of day; $Q_{UP,i}$ is daily sediment yield volume from the outlet in Scenario UP of day i; $Q_{PP/EP,i}$ is daily sediment yield volume from the outlet in Scenario PP or Scenario EP of day i; $\mathrm{Re}_{PP/EP,i}$ is daily relative effectiveness of controlling measures in Scenario PP or Scenario EP of day i.

4. Results

4. 1 *Overall geomorphic changes*

There were three panoramas at the end of each year in each scenario, which were classified into seven ranks by natural breaks for EleDiffs (Fig. 5): extreme erosion (-15-10 m), heavy erosion (-10--7 m), moderate erosion (-7--3 m), light erosion (-3--1

https://doi.org/10.5194/nhess-2022-195
Preprint. Discussion started: 11 July 2022

m), micro change (-1-1 m), light deposition (1-3 m), moderate deposition (3-7 m), heavy deposition (7-10 m), and extreme deposition (10-14 m). The erosion and deposition aggravated in a similar spatial pattern in all three scenarios. Erosion occurred mainly in the upper reaches of the main channel and the branches on both sides, among which the left branches were extremely serious, such as Qinggangping gully and Shicaozi gully. As shown in Fig. 5, the three scenarios appeared to have different distribution patterns, especially around the two dams. Statistically, the Scenario UP damaged 0.76 km^2 (5.4% of the total catchment), the PP affected 0.70 km^2 (5.0% of the total catchment), and the EP decreased the area to 0.61 km^2 (4.4% of the total catchment). The damaged area reduced gradually as the more controlling measures for loose solid materials.

In addition, the affected area of seven ranks changes showed different effects in the different scenarios. Erosion in the three scenarios was similar in that the light and the moderate erosion areas were more than the area of extreme and heavy erosion. The area of each erosion degree in UP was almost larger than that in PP and both larger than that in EP, except that the light erosion area in PP was slightly larger than that in the UP. For the deposition in the internal geography, the greater deposition depth, the less coverage of deposition. Especially, the extreme deposition area was slightly more than the area of the heavy deposition in UP. Further analysis showed that the extreme, moderate, and light deposition areas decreased to varying degrees in the order of UP, PP, and EP, and the heavy deposition areas showed the opposite trend, which mainly contributed to the blocking of dams and vegetation revetment.

https://doi.org/10.5194/nhess-2022-195
Preprint. Discussion started: 11 July 2022

Natural Hazards and Earth System Sciences
Discussions
Open Access

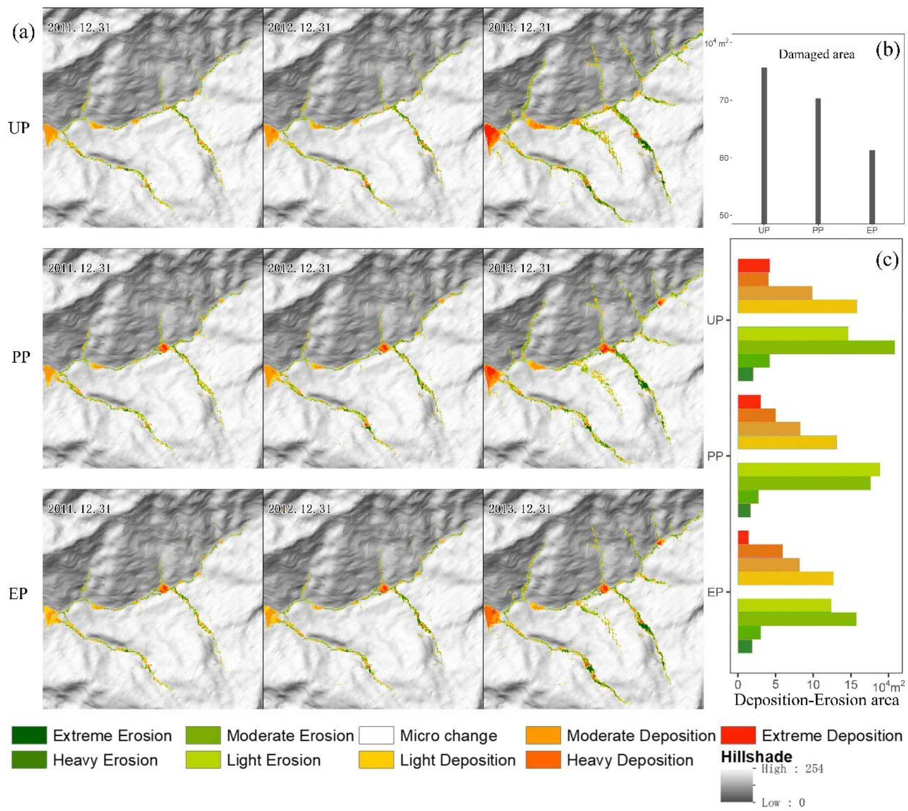

Fig. 5. (a) Simulated internal geomorphic changes over time for three scenarios; (b) the damaged area included deposition and erosion for three scenarios; (c) the final different ranks of deposition and erosion for three scenarios.

4. 2 *Details of key spots*

An amplified investigation of the controlling measures around their position detailed the differences in the three scenarios. Therefore, the upriver land panorama, containing two dams in Scenario PP and cooperating with extra biological measures in Scenario EP, was used to outline the affected area, measure the impacts on blocking sediment, and examine how the biological area helped to stabilize the slope. Similarly, the panorama of downriver land described the two levees in scenario EP escape from the debris, protecting the plow lands and buildings.

https://doi.org/10.5194/nhess-2022-195
Preprint. Discussion started: 11 July 2022

In the upriver reservoirs of the two dams (Fig. 6), the evident orange clusters indicated the accumulation in Scenario PP and EP, whereas erosion showed in green in the scenario UP. The area of accumulation blocked by dam 1 in EP was similar to PP's area while the accumulation in EP covered a larger range than that in PP blocked by dam 2. Further analysis (Fig. 7) about the depth of deposition blocked by two dams showed that the depth blocked by dam 2 was larger than that blocked by dam 1 in Scenario UP and PP. Whereas, the deposition depth blocked by dam 2 decreased to be slightly lower than that by dam 1 in Scenario EP. In Scenario PP, the sediment depth blocked by dam 1 was larger than the height of the dam body at the end of simulation time. Similarly, the accumulation blocked by dam 2 exceeded the dam height at last. In Scenario EP, both the reservoir areas of dam 1 and dam 2 were lower than the dams' height.

The materials produced from upriver tributary gullies varied in three scenarios by the extra biological protection measures. There yielded 14.4×10^4 m^3 loose materials in EP's biological protection area (solid lines in Fig. 6). In the same gullies, the loose materials were 27.1×10^4 m^3 and 16.9×10^4 m^3, respectively in Scenario UP and PP without biological protection. The vegetation revetment enhanced the sediment conservation based on the role of dam 1. In addition, the materials were carried mainly from the two gullies in the upriver of dam 2 and the downriver of biological protection area, which was inferred from the larger amount of erosion volumes in two gullies in each scenario (48.2×10^4 m^3, 42.5×10^4 m^{3,} and 35.2×10^4 m^3 in Scenario UP, PP, and EP).

https://doi.org/10.5194/nhess-2022-195
Preprint. Discussion started: 11 July 2022

362 In the downriver area, the levees had an important role in preventing debris and protecting the property. Compared with the accumulation in UP and PP without levees, the levees in EP blocked debris in the bend of the channel and protected the residents and cultivated land along the river.

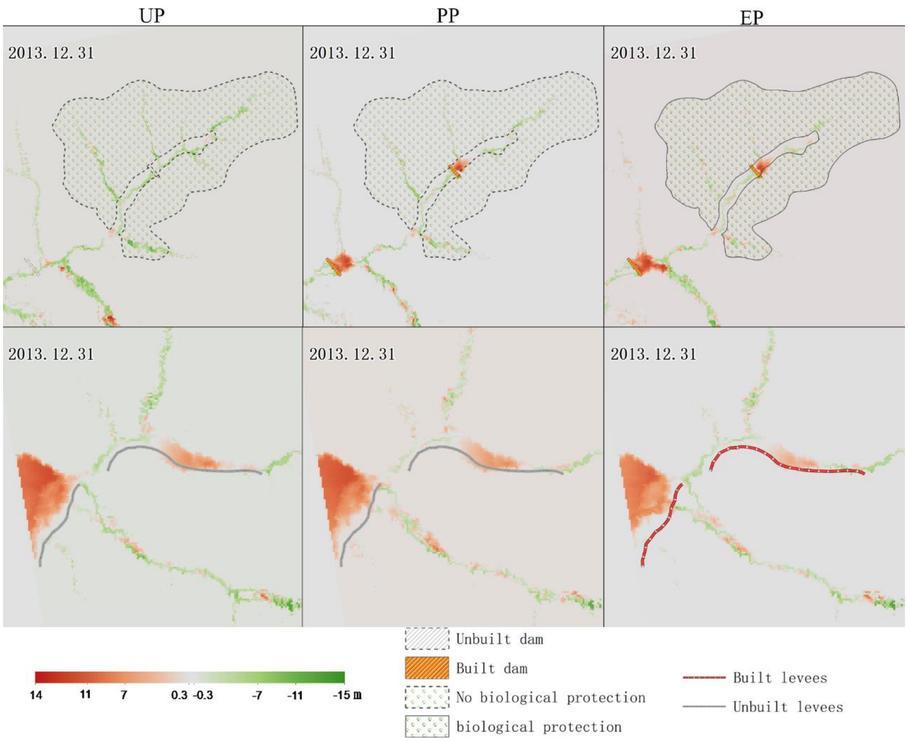

366

367 Fig. 6. The final detailed geomorphic changes in the key spots (the upriver dam 1, dam 2 in Scenario PP and EP and vegetation revetment in Scenario EP showed in the first row; the downriver levees in Scenario EP represent in the second row)

https://doi.org/10.5194/nhess-2022-195
Preprint. Discussion started: 11 July 2022

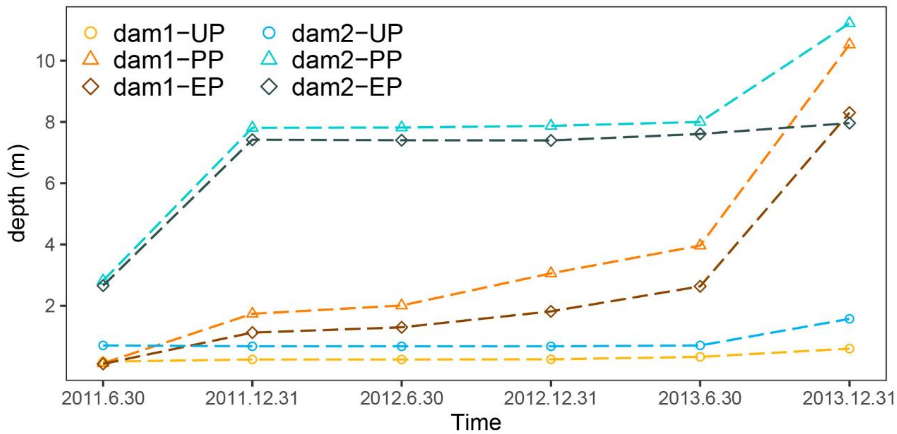

Fig. 7. The depth of deposited sediment blocked by dams in three scenarios

4. 3 *Divisional erosion and deposition*

We analyzed the source area, translation area, and deposit area by calculating the eroded and accumulated sediment volume. Fig. 8 shows the erosion and deposition distribution induced by rain over three years. The data showed similar phenomena in three scenarios, i.e., the eroded volume in the source area was less than that in the deposit area, and both were less than that in the translation area. The degree of deposition in the source area was less than that in the translation area, and the largest deposition was in the deposit area.

From the analysis of sediment conservation ability (see section 3.3) in each region controlled by different measures in three scenarios, the deposit area was the best at all times, and the source area was the worst. Dam 1 in the source area and Dam 2 in the translation area were so effective that the materials conservation ability increased by 138.1% and 52.5% in Scenario PP compared with Scenario UP, respectively (Table 2). What’s more, the mitigation measures with vegetation revetment and levees in Scenario EP worked better. The ability in the source area increased by 161.9%, and the levees helped increase by 3.49% compared with Scenario UP. Therefore, the dams

https://doi.org/10.5194/nhess-2022-195
Preprint. Discussion started: 11 July 2022

were most effective in blocking sediment, the vegetation revetment strengthened the conservation ability, and the levees worked mainly to prevent damage.

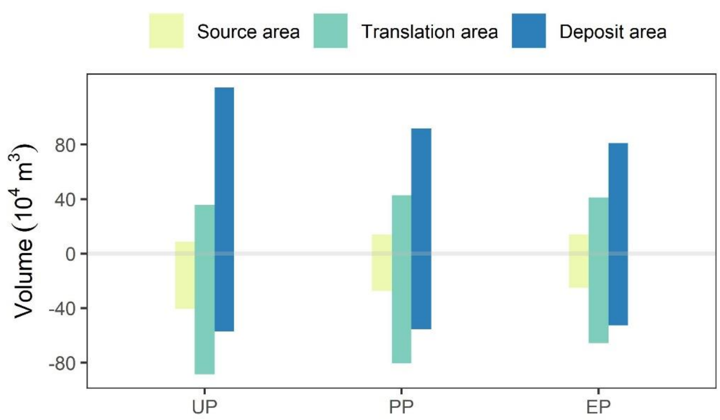

Fig. 8. The deposition and erosion volumes in different areas

Table 2 The sediment conservation ability

Region \ Scenario	UP	PP	EP
Source area	0.21	0.50	0.55
Translation area	0.40	0.61	0.62
Deposit area	0.86	0.86	0.89

4. 4 *Effectiveness assessment*

Fig. 9 presents the time series of cumulative sediment yield for each scenario according to the output file. The steep curve means the great increase of sediment and three increasing stages have high consistency with the rainfall intensity in three monsoons (May-September). The total sediment output in UP was the largest, about 30.4×10^4 m^3, and the total output in PP (26.3×10^4 m^3) was larger than that in EP (19.3×10^4 m^3). We used the formula mentioned in section 3.3 to calculate the relative efficiency of controlling measures by human intervention in PP and EP (Fig. 9b). Three distinct stages were clear for the effective degree between PP and EP. The stage

https://doi.org/10.5194/nhess-2022-195
Preprint. Discussion started: 11 July 2022

Natural Hazards and Earth System Sciences
Discussions
Open Access

I showed that the two dams in PP or two dams with two levees and vegetation protection in EP both controlled the sediment loss. Later stage II was an existing and peculiar period where the effect of enhanced protective measures in EP was not as good as that in PP after many simulation trials. In stage Ⅲ, the relative efficiency of the intervention measures in EP was greater than that in UP, which could achieve long-term effective and stable conservation of solid materials. What's more, the relative efficiency values in PP's stage Ⅲ showed a decreasing trend, whereas the values declined indeterminately in EP's stage Ⅲ because of the slight increase in values at the end of the simulation. In general, the engineering works in controlling sediment transport were efficient, and it would be better at protecting the fragile environment effectively with other intervention measures like vegetation revetment and levees. In addition, the effectiveness of conservation and mitigation would decrease with time.

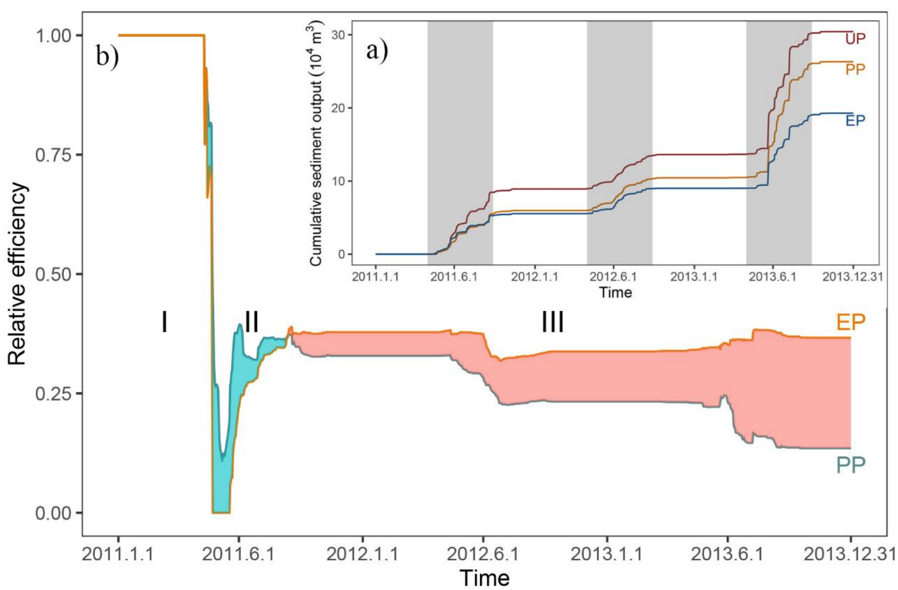

Fig. 9. a) showing the output cumulative sediment over time (grey region highlighting three monsoons); b) showing the relative efficiency of scenario UP and EP compared with the UP (green region representing PP more effective than EP and red region standing the opposite)

https://doi.org/10.5194/nhess-2022-195
Preprint. Discussion started: 11 July 2022

Natural Hazards and Earth System Sciences
Open Access
EGU
Discussions

5. Discussion

5. 1 *Reliability and uncertainty*

Reliability and uncertainty deserve a discussion for understanding and implementing the simulation results in most geographical analyses and modeling processes (Yeh and Li, 2006). Comparative simulation tests using the C-L tool suggested a complex spatial and temporal evolution of sediment transport. In addition, the tool demonstrated that the efficiency according to space and time varied in scenarios, which differed in control measures conducted on the mountainous areas that are susceptible to secondary geo-hazards. In this study, for the parameters involving geological conditions, we cited local research and comprehensive parameter sensitivity papers; we downscaled the daily rainfall sequence into hourly rainfall data collected in 2016 for every year because the total rainfall and intensity were identified as 'normal year' rainfall in 2016 (Xie et al., 2018). For the generated input data, although the intensity and event time would not be the same as the actual value, the realization of total rainfall in three different years suggested reasonable differences.

In addition, the optimal simulation result was decided according to the sediment depth in dam reservoirs and output between simulation and actual measurement from field survey or literature research. Fig. 10a shows the sediment distribution blocked by dam 1 in August 2012; the distance from the dam crest to the deposition level was up to 7 m, which suggested that the buried dam depth was nearly 3 m (dam height: 10 m). Therefore, the 3 m-depth simulation result of PP in the same moment found in Fig. 6 (see section 4.2) was consistent with the actual value. In October 2013, the same location collected by photo in Fig. 10b showed that the reservoir was full of ma-

https://doi.org/10.5194/nhess-2022-195
Preprint. Discussion started: 11 July 2022

Natural Hazards and Earth System Sciences
Discussions
Open Access
EGU

terials, which were equal to the simulation depth of more than 10 m in Fig. 6. Conversely, the sediment yield in 2013 was up to $29.5 \times 10^4 m^3$ (Feng et al., 2017), which was from mainly the Shicouzi gully. Coincidentally but more scientifically, the apparent new erosion that occurred in 2013 in Shicouzi (Fig. 4) suggested the disaster history was rebuilt successfully by simulation, and the erosion volume in Shicouzi was 20.6×10^4 m^3. Therefore, it was reasonable that the simulation of eroded materials from Shicouzi accounted for 70% of the sediment from the left branch gully.

Fig. 10. The photos of dam 1 reservoir (the red single arrows showing the azimuth angle and the double arrows showing the height of the dam body)

5. 2 *Short-medium term problem*

We used an ingenious and simple method to build the dams and levees in the simulation by increasing the elevation in the expected location and assuming that it could not be eroded (see https://sourceforge.net/projects/caesar-lisflood/). This method proved to be experimentally feasible (Gioia and Schiattarella, 2020; Poeppl et al., 2019). The rigid dam and levee body embedded in the model would not be broken, and the effect would not be weakening, so the result of geo-hazard risk assessment would be reduced to some extent. Although the fast and large amount of moving debris triggered a tremendous impact in the simulation, the tools could not simulate the

https://doi.org/10.5194/nhess-2022-195
Preprint. Discussion started: 11 July 2022

geo-hazard chain links and would ignore the fierce attack on the environment and facilities downstream. Some typical geo-hazard chains were focused on the specified event in a short time and recreated the hazard lifecycle using physical and mechanical models (Fan et al., 2019). We concentrated on the effectiveness of mitigation measures in the short-medium term, which is different from those in space-time scales and purposes. Therefore, the three-year simulation time made it underestimated risk assessment, and a success to simulate the effect of mitigation measures compared with the actual result in this study.

5. 3 *Sediment transport patterns*

Different from the typical debris flow research, where three divided areas get their names for the materials process, the simulation result demonstrated the loose solid materials from the source area sliding to the resting area were the least among the three regions, even for the scenario UP (unprotected landscapes). The sediment transport patterns change considerably and two reasonable descriptions are as follows. First, the abundant loose solid materials formed by the strong earthquake have stabilized generally since 2008's debris flow (details in Table 1). Second, the long, deep, and steep gullies are mainly located in the translation area (Yaogouli, Shicouzi, Yangjiashan) and deposit area (Qinggangping). Thus, the large erodible area and the poor topographic conditions destroyed the circulation and deposit area more than the source area. Just as Fig. 11 shows, the movement of the materials occurred mainly in the branches in the circulation and deposit area.

https://doi.org/10.5194/nhess-2022-195
Preprint. Discussion started: 11 July 2022

Natural Hazards and Earth System Sciences Discussions

Fig. 11. Photos showing hazards sites in different areas: a) the source area, b) the deposit area, c) and d) the translation area

5. 4 *Long-term trials*

In the future warmer world with more water vapor in the atmosphere, precipitation extremes will be intensified, increasing the likelihood of extreme and intense rainfall (East and Sankey, 2020). Then sequential increased fluvial transport capacity and erosion would accelerate geomorphic changes. With increased uncertainty of precipitation and temperature, future work about landscape evolution of three scenarios will help to understand long timescale effectiveness of intervention measures. We randomly selected one of the 50 repeat datasets downscaled by Li et al., (2020), which were generated in 2013-2025 and RCP 4.5 emission scenario from NEX-GDDP (spatial resolution: 0.25°×0.25°, temporal resolution: daily) to simulate the effectiveness in three scenarios. The result (Fig. 12) illustrated that stage III (stable stage started on the 161st day, in which Scenario EP's intervention measures were more effective) was more than stage I and II, which were only in the beginning. The relative effectiveness

https://doi.org/10.5194/nhess-2022-195
Preprint. Discussion started: 11 July 2022

Natural Hazards and Earth System Sciences
Open Access
Discussions

in both scenarios decreased gradually and the curve went down faster in PP than that in EP.

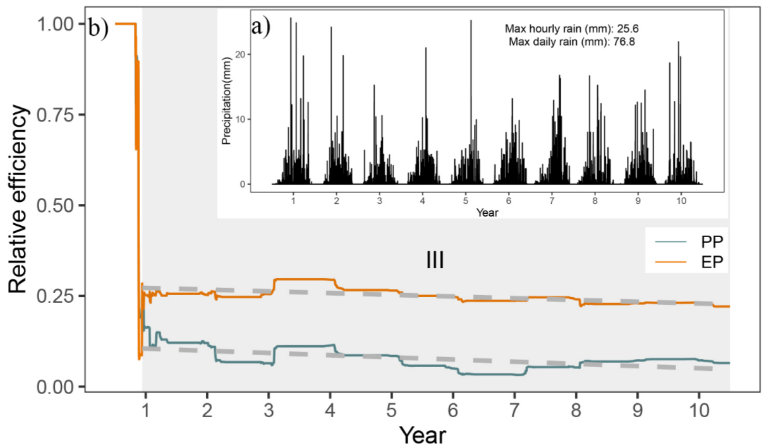

Fig. 12. a) Rainfall downscaled from stochastic future rainfall; b) the relative efficiency changes over ten years (grey region highlighting stage III, and the grey dashed lines indicated the linear fitting curve)

6. Conclusions

We have four key findings. First, the comparative scenario simulations showed that mitigation measures in scenario PP (containing two blocking dams) and scenario EP (incorporating biological processing in the source area with two dams) were effective in reducing erosion, controlling sediment output, and protecting property from damage in post-earthquake fragile mountains prone to secondary geo-hazards. Erosion had a high consistency with the monsoons (May-September) and was mainly in the upper reaches and the left branches of the main gully. The two dams have blocked the upstream sediment successfully and the levees had an important role in preventing the debris shocking, and burial of the residents and cultivated land along the river. In addition, the decrement in EP suggested the accumulated materials blocked by dams upgrade a slope upstream in turn. What's more, model embedded quantification of vege-

https://doi.org/10.5194/nhess-2022-195
Preprint. Discussion started: 11 July 2022

tation revetment showed that the sediment yielded decreased 5 times as much as scenario UP, which contributed to that the vegetation cover enhanced precipitation infiltration and reduced flow velocity.

Second, reasonable and comprehensive treatment methods for a mountainous area with abundant solid materials reduced internal geomorphology changes and sediment output. The areas of erosion and deposition varied in degree decreased in EP compared with PP, except for heavy deposition. Then both the internal damaged area and the erosion volume in EP were less than in PP. In addition, the reduced volume of erosion in the source area between EP and PP was larger than the deposition volume suggesting the vegetation protection was effective in EP. Conversely, three years later, the simulated depth of accumulation blocked by dam 1 and dam 2 was greater than the height of the dams in PP, whereas only the depth deposited in the upriver of dam 2 was greater than the dam height. Moreover, the present intervention measures are not adequate to reduce erosion and should be combined with dredging work.

Third, zonal statistics of the volumes of erosion and deposition in the source area, translation area, and deposit area demonstrated that the characteristics of sediment transport patterns changed considerably. The conservation ability in the deposit area was the best at all times, and the source area was the worst. Dam 1 in the source area and dam 2 in the translation area worked so well that the materials conservation ability increased by 138.1% and 52.5% compared with the scenario without any intervention method. With the extra help of vegetation revetment, the ability in the source area increased by 161.9%, and the levees helped the deposit area increase by 3.49%.

Fourth, the two types of effectiveness found in the sediment output simulated under Scenario PP and EP compared with Scenario UP were divided into three apparent stages with a general downward trend. The first stage was completely effective in both

PP and EP, whereas stage Ⅱ was a peculiar period in which the effect in EP was not as good as that in PP, which would be caused by the increasing complexity of the model. Lastly, steady effectiveness would be sustainable as shown in stage Ⅲ, in which the effectiveness simulated in EP with vegetation revetment and levees was greater than that in PP.

Taking long-term effectiveness and the function of vegetation into consideration for mitigation measures is more helpful to understand the efficiency. More works should be carried out to explore, especially with the increased likelihood of extreme and intense rainfall in the future.

Declaration of interest statement

The authors declare that they have no known competing financial interests or personal relationships that could have appeared to influence the work reported in this paper.

Author contribution

Di Wang: Conceptualization, Methodology, Software, Writing-original draft preparation. Ming Wang and Kai Liu: Supervision, Methodology, Writing- Reviewing and Editing, Validation.

Acknowledgments

This research was supported by the National Key Research and Development Plan (2017YFC1502902). The financial support is highly appreciated. The authors would also like to thank Professor Tom Coulthard and his team for their excellent work on the freely available C-L model (https://sourceforge.net/projects/ caesar-lisflood).

https://doi.org/10.5194/nhess-2022-195
Preprint. Discussion started: 11 July 2022

Reference

Arcement, G. J., and Schneider, V. R.: Guide for selecting Manning's roughness coefficients for natural channels and flood plains, United States Geological Survey Water-Suply Paper 2339, https://doi.org/https://doi.org/10.3133/wsp2339, 1989.

Bates, P. D., Horritt, M. S., and Fewtrell, T. J., A simple inertial formulation of the shallow water equations for efficient two-dimensional flood inundation modelling, J. Hydrol., 387(1–2), 33–45, https://doi.org/10.1016/j.jhydrol.2010.03.027, 2010.

Batty, M., Couclelis, H., and Eichen, M.: Urban systems as cellular automata, Environ Plan B Urban Anal City Sci, 24(2), 159–305, https://doi.org/10.1068/b240159, 1997.

Batty, M., and Xie, Y.: Possible urban automata, Environ Plann B Plann Des, 24(2), 175–192. https://doi.org/10.1068/b240175, 1997.

Beven, K. J., and Kirkby, M. J.: A physically based, variable contributing area model of basin hydrology, Hydrol Sci J, 24(1), 43–69, https://doi.org/10.1080/02626667909491834, 1979.

Chen, N., Zhou, H., Lu, Y., Yang, L., and Lv, L.: Analysis of benefits of debris flow control projects in southwest mountains areas of China (In Chinese). Journal of Chengdu University of Technology (Science and Technology Edition), 40(1), 50–58, https://doi.org/10.3969/j.issn.1671-9727.2013.01.008, 2013.

Cong, K., Li, R., and Bi, Y.: Benefit evaluation of debris flow control engineering based on the FLO-2D model (In Chinese), Northwestern Geology, 52(3), https://doi.org/10.19751/j.cnki.61-1149/p.2019.03.019, 2019.

Couclelis, H.: From cellular automata to urban models: new principles for model development and implementation, Environ Plann B Plann Des, 24(2), 165–174, https://doi.org/10.1068/b240165, 1997.

Coulthard, T J, Macklin, M. G., and Kirkby, M. J.: A cellular model of Holocene upland river basin and alluvial fan evolution, Earth Surf Process Landf, 27(3), 269–288, https://doi.org/10.1002/esp.318, 2002.

Coulthard, Tom J., Hancock, G. R., and Lowry, J. B. C.: Modelling soil erosion with a downscaled landscape evolution model, Earth Surf Process Landf, 37(10), 1046–1055, https://doi.org/10.1002/esp.3226, 2012.

Coulthard, Tom J, Neal, J. C., Bates, P. D., Ramirez, J., de Almeida, G. A. M., and Hancock, G. R.: Integrating the LISFLOOD-FP 2D hydrodynamic model with the CAESAR model: Implications for modelling landscape evolution, Earth Surf Process Landf, 38(15), 1897–1906, https://doi.org/10.1002/esp.3478, 2013.

Cui, P., Zhou, G. G. D., Zhu, X. H., and Zhang, J. Q.: Scale amplification of natural debris flows caused by cascading landslide dam failures. Geomorphology (Amst) , 182(August 2010), 173–189, https://doi.org/10.1016/j.geomorph.2012.11.009, 2013.

East, A. E., and Sankey, J. B.: Geomorphic and Sedimentary Effects of Modern Climate Change: Current and Anticipated Future Conditions in the Western United States. Rev. Geophys., 58(4), https://doi.org/10.1029/2019RG000692, 2020.

Fan, X., Yang, F., Siva Subramanian, S., Xu, Q., Feng, Z., Mavrouli, O., Peng, M., Ouyang, C., Jansen, J. D., and Huang, R.: Prediction of a multi-hazard chain by an integrated numerical simulation approach: the Baige landslide, Jinsha River,

https://doi.org/10.5194/nhess-2022-195
Preprint. Discussion started: 11 July 2022

China, Landslides, 17(1), 147–164, https://doi.org/10.1007/s10346-019-01313-5, 2019.

Feng, W., He, S., Liu, Z., Yi, X., and Bai, H.: Features of debris flows and their engineering control effects at xinping gully of pingwu county (In Chinese) , Journal of Engineering Geology, 25(3), 794–805, https://doi.org/10.13544/j.cnki.jeg.2017.03.027, 2017.

Gioia, D., and Schiattarella, M.: Modeling Short-Term Landscape Modification and Sedimentary Budget Induced by Dam Removal: Insights from LEM Application, Appl. Sci., 10, 7697, https://doi.org/10.3390/app10217697, 2020.

Goldberg, D. E. Genetic Algorithms in Search, Optimization, and Machine Learning, 35, 2, Addison-Wesley Longman Publishing Co., Inc, https://doi.org/10.1007/BF01920603, 1989.

Guo, Q., Xiao, J., and Guan, X.: The characteristics of debris flow activities and its optimal timing for the control in Shikan River Basin Pingwu Country (In Chinese), The Chinese Journal of Geological Hazard and Control, 29(115(03)), 37–43, https://doi.org/10.16031/j.cnki.issn.1003-8035.2018.03.05, 2018.

Hancock, G. R., Verdon-Kidd, D., and Lowry, J. B. C.: Soil erosion predictions from a landscape evolution model – An assessment of a post-mining landform using spatial climate change analogues, Sci. Total Environ, 601–602, 109–121, https://doi.org/10.1016/j.scitotenv.2017.04.038, 2017.

Highland, L. M., and Bobrowsky, P.: The landslide Handbook - A guide to understanding landslides, In US Geological Survey Circular, 1325, https://doi.org/10.3133/cir1325, 2008.

Huang, R, Geohazard assessment of the Wenchuan earthquake (In Chinese), Science Press, Beijing, 2009.

J.B.C.Lowry, M.Narayan, G.R.Hancock, K.G.Evans, and K.G.Evans.: Understanding post-mining landforms: Utilising pre-mine geomorphology to improve rehabilitation outcomes, Geomorphology (Amst), 328, 93–107, https://doi.org/10.1016/j.geomorph.2018.11.027, 2019.

Lee, T., and Jeong, C.: Nonparametric statistical temporal downscaling of daily precipitation to hourly precipitation and implications for climate change scenarios, J. Hydrol., 510, 182–196, https://doi.org/10.1016/j.jhydrol.2013.12.027, 2014.

Li, C., Wang, M., and Liu, K.: A decadal evolution of landslides and debris flows after the Wenchuan earthquake, Geomorphology (Amst), 323, 1–12, https://doi.org/10.1016/j.geomorph.2018.09.010, 2018.

Li, C., Wang, M., Liu, K., and Coulthard, T. J., Landscape evolution of the Wenchuan earthquake-stricken area in response to future climate change, J J. Hydrol., 590(June), 125244, https://doi.org/10.1016/j.jhydrol.2020.125244, 2020.

Poeppl, R. E., Coulthard, T., Keesstra, S. D., and Keiler, M.: Modeling the impact of dam removal on channel evolution and sediment delivery in a multiple dam setting, Int. J. Sediment Res, 34(6), 537–549, https://doi.org/10.1016/j.ijsrc.2019.06.001, 2019.

Saynor, M. J., Lowry, J. B. C., and Boyden, J. M.: Assessment of rip lines using CAESAR-Lisflood on a trial landform at the Ranger Uranium Mine, L Land Degrad Dev, 30(5), 504–514, https://doi.org/10.1002/ldr.3242, 2019.

Skinner, C. J., Coulthard, T. J., Schwanghart, W., Van De Wiel, M. J., and Hancock, G. Global sensitivity analysis of parameter uncertainty in landscape evolution models, Geosci Model Dev, 11(12), 4873–4888, https://doi.org/https://doi.org/10.5194/gmd-11-4873-2018, 2018.

https://doi.org/10.5194/nhess-2022-195
Preprint. Discussion started: 11 July 2022

Natural Hazards and Earth System Sciences
Discussions

Slingerland, N., Beier, N., and Wilson, G.: Stress testing geomorphic and traditional tailings dam designs for closure using a landscape evolution model, Proceedings of the 13th International Conference on Mine Closure, 1533–1544, https://doi.org/10.36487/ACG_rep/1915_120_Slingerland, 2019.

Thomson, H., and Chandler, L.: Tailings storage facility landform evolution modelling, Proceedings of the 13th International Conference on Mine Closure, 385–396, https://doi.org/10.36487/ACG_rep/1915_31_Thomson, 2019.

Van De Wiel, M. J., Coulthard, T. J., Macklin, M. G., and Lewin, J.: Embedding reach-scale fluvial dynamics within the CAESAR cellular automaton landscape evolution model, Geomorphology (Amst), 90(3), 283–301, https://doi.org/10.1016/j.geomorph.2006.10.024, 2007.

Wang, M., Liu, M., Yang, S., and Shi, P.: Incorporating Triggering and Environmental Factors in the Analysis of Earthquake-Induced Landslide Hazards, Int. J. Disaster Risk Sci., 5(2), 125–135, https://doi.org/10.1007/s13753-014-0020-7, 2014.

Wang, M., Yang, W., Shi, P., Xu, C., and Liu, L.: Diagnosis of vegetation recovery in mountainous regions after the wenchuan earthquake, I IEEE J Sel Top Appl Earth Obs Remote Sens, 7(7), 3029–3037, https://doi.org/10.1109/JSTARS.2014.2327794, 2014.

Wang, N., Han, B., Pang, Q., and Yu, Z.: Post-evaluation model on effectiveness of debris flow control (In Chinese). Journal of Engineering Geology, 23(2), 219–226, https://doi.org/10.13544/j.cnki.jeg.2015.02.005, 2015.

Xie, J., Wang, M., Liu, K., and Coulthard, T. J.: Modeling sediment movement and channel response to rainfall variability after a major earthquake, Geomorphology (Amst), 320, 18–32, https://doi.org/10.1016/j.geomorph.2018.07.022, 2018.

Yeh, A. G. O., and Li, X.: Errors and uncertainties in urban cellular automata, Comput Environ Urban Syst, 30(1), 10–28, https://doi.org/10.1016/j.compenvurbsys.2004.05.007, 2006.

Yu, B., Yang, Y., Su, Y., Huang, W., and Wang, G.: Research on the giant debris flow hazards in Zhouqu County, Gansu Province on August 7, 2010 (In Chinese), Journal of Engineering Geology, 18(4), 437–444, https://doi.org/10.3969/j.issn.1004-9665.2010.04.001, 2010.

Zhang, L., and Liang, K.: Research on economic benefit evaluation of the prevention and cure project for debris flow (In Chinese), The Chinese Journal of Geological Hazard and Control, 16(3), 48–53, https://doi.org/10.3969/j.issn.1003-8035.2005.03.011, 2005.

Zhang, X., Wang, M., Liu, K., Xie, J., and Xu, H.: Using NDVI time series to diagnose vegetation recovery after major earthquake based on dynamic time warping and lower bound distance, Ecol. Indic.,94(June), 52–61, https://doi.org/10.1016/j.ecolind.2018.06.026, 2018.

Zhao, C., Liang, J., Xie, Z., She, T., and Zhang, S.: Remote sensing dynamic analysis of debris flow activity characteristics in strong earthquake area of Wenchuan earthquake 10 years after earthquake-A case study of shikan river watershed of pingwu county (In Chinese), Journal of Catastrophology, 34(4), 222–227, https://doi.org/10.3969/j.issn.1000－811X.2019.04.038, 2019.

Zhou, H., Chen, N., Lu, Y., and Li, B.: Control Effectiveness of Check Dams in Debris Flow Gully: A Case of Huashiban Gully in Earthquake Worst-stricken Area, Beichuan County (In Chinese), Journal of Mountain Science, 30(3), 347–354, (https://doi.org/10.3969/j.issn.1008-2786.2012.03.015, 2012.